

VIP Very Important Paper

Nanocrystalline H-RTH Zeolite: An Efficient Catalyst for the Low-Temperature Dehydration of Ethanol to Ethene

Jeong Hwan Lee, Sujin Lee, and Suk Bong Hong*^[a]

The low-temperature dehydration of bioethanol is an environmentally benign route to ethene production. Here we compare the catalytic properties of a series of cage-based small-pore zeolites with different framework structures, acid strengths, and/or crystallite sizes for ethanol dehydration at 200 °C under wet conditions (H₂O/EtOH=0.2). Among the zeolites studied here, nanocrystalline H-RTH was found to be considerably more effective than H-mordenite, the best catalyst for this reaction known to date, which can be rationalized by product shape selectivity. Whereas the acidity of this zeolite also plays a crucial role in selectively forming ethene, its nanocrystallinity is primarily responsible for the observed high catalyst durability.

Ethene, one of the most basic chemical building blocks in petrochemistry, is widely used for the production of polyethylene, as well as other chemical products, such as ethylene oxide, ethylene dichloride, and ethylbenzene.^[1] Currently, ethene production is dominated by the steam cracking of hydrocarbons from fossil fuels, which inevitably accompanies the emission of a huge amount of CO₂ (1.5 times ethene in weight), a major contributor to the greenhouse effect. Alternatively, ethene could be produced via the acid-catalyzed dehydration of ethanol (i.e., the removal of its hydroxyl group and a vicinal proton). Given ever-intensifying global warming, considerable attention is being given to finding more environmentally benign routes based on renewable feedstocks, as well as fermentation technology development for the mass production of bioethanol, which in turn has led to the bio-based manufacture of ethene.^[2] However, the fermentative route to produce bioethanol results in mixtures with approximately 95 wt% water, which should be further concentrated through distillation.

Because ethanol and water can form a binary azeotrope system (95.63 wt% ethanol), highly energy-consuming processes like extractive and/or azeotropic distillations cannot be avoided to produce high-purity ethanol above the azeotropic composition.^[3] Therefore, the direct use of hydrous ethanol below the azeotropic composition is one of the main criteria

for production of ethene from bioethanol to be environmentally and industrially friendly by avoiding a strenuous separation process. A wide variety of solid acid catalysts, including phosphated metal oxides, heteropolyacids, and zeolitic materials, have been tested for the dehydration of ethanol to ethene.^[4] Owing to the uniformly defined pore structures with distinctive shapes, as well as the intrinsic acidic properties, zeolites and related molecular sieves hold a firm place in numerous acid-catalyzed reactions. Among those catalysts studied so far, the large-pore zeolite H-mordenite (framework type MOR) has been known to be the most selective for ethene formation below 250 °C, because of its confined 8-membered ring side pockets within which the creation of bulky ethanol dimers, a prerequisite for diethylether (DEE) formation, can be restricted.^[5]

We have recently shown that although the channel-based small-pore zeolite H-EU-12 (ETL) gives a low ethanol conversion at 200 °C, it is quite selective for ethene formation.^[6] Given the relatively smaller kinetic diameter (4.2 vs. 5.4 Å) of ethene compared to DEE,^[7] we attributed the catalytic behavior of H-EU-12 to product shape selectivity. According to the microkinetic modeling study by Alexopoulos et al.,^[8] on the other hand, the bimolecular pathway via DEE decomposition for ethene formation at low temperatures (e.g., 227 °C) is energetically more favorable than the monomolecular pathway. This led us to consider the possibility that cage-based small-pore zeolites could be both active and selective for ethanol dehydration, because the formation of ethanol dimers should be less feasible in channel-based small-pore zeolites. Here we report the catalytic properties of a series of such zeolites with different framework topologies [i.e., H-levyne (LEV), H-SSZ-13 and H-SAPO-34 (CHA), H-SSZ-39 (AEI), H-RTH, and H-LTA), acid properties, and/or crystal sizes for low-temperature ethanol dehydration under wet conditions (H₂O/EtOH=0.2). Nanocrystalline H-RTH was found to be considerably more active and selective than H-mordenite, known as the most active catalyst for this reaction.

All small-pore zeolites employed in this work, the crystallographic pore and cavity dimensions and the framework structures of which are given in Table 1 and Figure 1, respectively, were synthesized and converted into their proton form following the procedures described in the literature.^[6,9] For comparison, H-mordenite (Si/Al=10) was obtained from Tosoh. Powder X-ray diffraction measurements (Figure S1 in the Supporting Information) reveal that each small-pore material synthesized is highly crystalline and phase pure,^[10] which can be further supported by the N₂ Brunauer–Emmett–Teller (BET) surface area data in Table 2. Also, no noticeable structural collapse is observed even after ethanol dehydration under wet condi-

[a] J. H. Lee, S. Lee, Prof. S. B. Hong
Center for Ordered Nanoporous Materials Synthesis, Division of Environmental Science and Engineering
Pohang University of Science and Technology (POSTECH)
Pohang, 37673 (Korea)
E-mail: sbhong@postech.ac.kr

 Supporting Information and the ORCID identification number(s) for the author(s) of this article can be found under:
<https://doi.org/10.1002/cssc.201800864>.

Table 1. Structural features of zeolite catalysts with different pore topologies.

Catalyst	IZA code	Pore topology	8-Ring pore size dimensions [Å]	area ^[a] [Å ²]	Channel intersection [Å]	Cavity size dimensions [Å]	volume ^[b] [Å ³]
H-EU-12	ETL	2D, 8-rings	2.7×5.0 3.3×4.8 2.8×4.6	10.6 12.4 10.1	6.7	–	–
H-levyne	LEV	2D, 8-rings	3.6×4.8	13.6	–	6.9×6.9×7.2	180
H-SSZ-13	CHA	3D, 8-rings	3.8×3.8	11.3	–	8.4×8.2×8.2	300
H-SAPO-34	CHA	3D, 8-rings	3.8×3.8	11.3	–	8.4×8.2×8.2	300
H-SSZ-39	AEI	3D, 8-rings	3.8×3.8	11.3	–	7.0×8.5×10.5	330
H-RTH	RTH	2D, 8-rings	2.5×5.6 3.8×4.1	11.0 12.2	–	10.4×11.0×9.0	540
H-LTA	LTA	3D, 8-rings	4.1×4.1	13.2	–	11.4×11.4×11.4	780
H-mordenite	MOR	12- and 8-rings + side pockets	6.5×7.0 ^[c] 2.6×5.7	– 11.6	–	–	–

[a] The pore area was calculated using the equation $A = \pi ab/4$, where A , a , and b are the pore area and the shortest and longest pore diameters, respectively. The pores in each zeolite are assumed to be ideally circular or elliptical in shape. [b] Calculated using the equation $V = \pi abc/6$, where V , a , b , and c are volume, width, length, and height of cage, respectively. All the cages are assumed to be ideally ellipsoidal in shape. [c] 12-ring pore size.

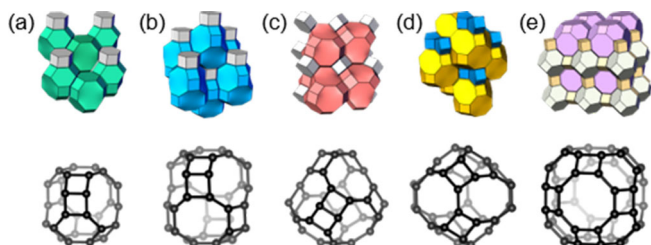


Figure 1. (a) LEV, (b) CHA, (c) AEI, (d) RTH, and (e) LTA structures. Given below is the largest cage in each structure.

tions ($\text{H}_2\text{O}/\text{EtOH} = 0.2$) at 200°C for 10 h on stream. ^{27}Al magic-angle spinning (MAS) NMR spectroscopy indicates that the extent of dealumination in all catalysts during ethanol dehydration in wet conditions is not severe (Figure S2). The characterization data in Table 2 and Figure 2 show that two of them, denoted as H-SSZ-13(II) and H-RTH(II), are nanocrystalline in nature.

Figure 3 shows the NH_3 temperature-programmed desorption (TPD) profiles obtained for the ten zeolite catalysts with

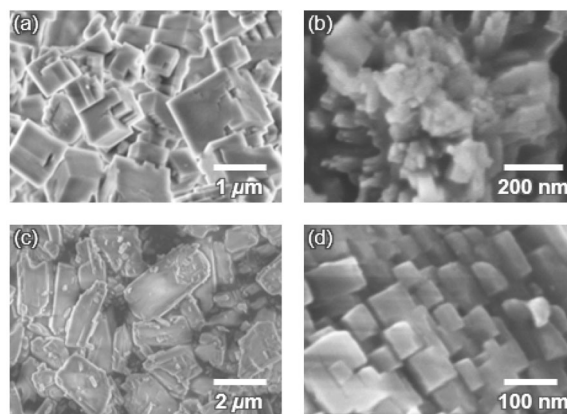


Figure 2. FE-SEM images of (a) H-SSZ-13(I), (b) H-SSZ-13(II), (c) H-RTH(I), and (d) H-RTH(II).

different framework structures, compositions, and/or crystallite sizes. Whereas all the TPD profiles, except those from H-levyne and H-SAPO-34, can be deconvoluted into three NH_3 desorp-

Table 2. Physical properties of zeolite catalysts.

Catalyst	Si/Al ratio ^[a]	Crystal shape	Avg. crystal size ^[b] [μm]	N_2 BET surface area ^[c] [m^2g^{-1}]			Organics deposited ^[d] [wt %]
				microporous	external	total	
H-EU-12	9.6	needles	0.1×1.0	210	170	380	4.8
H-levyne	7.9	overlapped cuboids	0.5–1.0	490	40	530	12.2
H-SSZ-13(I)	14	overlapped cuboids	0.5–1.0	580	80	660	6.8 (10.9)
H-SSZ-13(II)	19	irregular spherulites	0.03–0.06	470	130	600	5.3 (7.6)
H-SAPO-34	9.3 ^[e]	overlapped cuboids	0.5	450	70	520	4.8
H-SSZ-39	7.6	overlapped plates	0.5×0.5×0.1	590	60	650	12.4 (18.3)
H-RTH(I)	9.6	rectangular plates	0.5×2.0×0.1	580	80	660	10.1 (17.2)
H-RTH(II)	10	rods	0.05×0.05×0.10	430	120	550	11.2 (12.8)
H-LTA	11	overlapped cuboids	0.5–1.5	770	80	850	7.9
H-mordenite	10	rods	0.3×1.0	570	50	620	5.4 (8.4)

[a] Determined by elemental analysis. [b] Determined by FE-SEM. [c] Calculated from N_2 adsorption data. [d] Determined from TGA/DTA after ethanol dehydration at 200°C and 0.64 h^{-1} WHSV under wet conditions ($\text{H}_2\text{O}/\text{EtOH} = 0.2$) for 10 h on stream. The values in parentheses are the amount of organics deposited during the reaction at the same temperature but at a higher WHSV (1.92 h^{-1}) for 50 h on stream. [e] The (Al+P)/Si ratio.

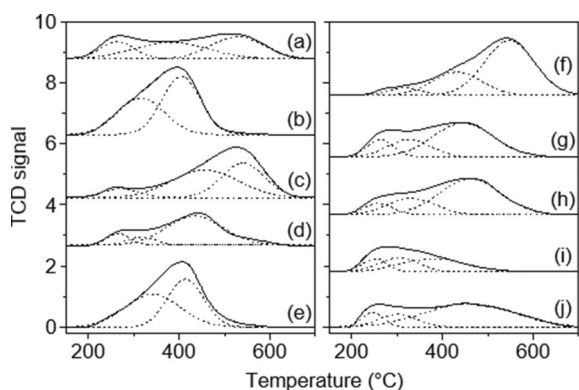


Figure 3. NH_3 TPD profiles from (a) H-EU-12, (b) H-levyene, (c) H-SSZ-13(I), (d) H-SSZ-13(II), (e) H-SAPO-34, (f) H-SSZ-39, (g) H-RTH(I), (h) H-RTH(II), (i) H-LTA, and (j) H-mordenite.

tion peaks, the concentration and strength distributions of the deconvoluted components are different from one another. As shown in Figure 3, the profiles for H-levyene, H-SAPO-34, and H-LTA exhibit no noticeable desorption peak maxima at temperatures higher than 450°C , indicating the lack of strong acid sites. Additionally, H-SSZ-13(I) and H-SSZ-13(II) with different bulk Si/Al ratios (14 vs. 19) and crystal sizes (0.8 vs. $\leq 0.06 \mu\text{m}$) exhibit quite different acidities; the temperature maximum (540 vs. 440°C) of the high-temperature desorption peak is significantly larger for the microcrystalline H-SSZ-13(I) than for the nanocrystalline H-SSZ-13(II). However, the temperature maximum (440 vs. 410°C) was found to be somewhat higher for H-SSZ-13(II) than for H-SAPO-34 with the same framework topology (CHA). Similar temperature maxima of the high-temperature desorption peak as that of H-SSZ-13(I) are also observable from H-EU-12 and H-SSZ-39.

It is also remarkable that the high-temperature NH_3 desorption peak from H-SSZ-39 is approximately 1.7 times stronger than that from H-SSZ-13(I). This explains why the former catalyst has a higher amount (12 vs. 7 wt%) of organic deposits than the latter catalyst when reacted with ethanol at 200°C for

10 h on stream (Table 2). On the other hand, the NH_3 TPD profiles for microcrystalline H-RTH(I) and nanocrystalline H-RTH(II) with almost the same Si/Al ratios (9.6 vs. 10) are characterized by rather similar acid densities and strength distributions. Therefore, the catalytic results from these two zeolites should display a crystal size effect. We also note that the temperature maximum (470°C) of their high-temperature desorption peaks are similar to that of H-mordenite with intersecting 12- and 8-ring channels.

Figure 4 shows ethene and DEE yields as a function of time on stream (TOS) in ethanol dehydration over H-EU-12, H-levyene, H-SSZ-13(I), H-SSZ-13(II), H-SAPO-34, H-SSZ-39, H-RTH(I), H-RTH(II), H-LTA, and H-mordenite measured at 200°C and weight hourly space velocity (WHSV) of 0.64 h^{-1} in the presence of water vapor ($\text{H}_2\text{O}/\text{EtOH} = 0.2$). As expected from the low reaction temperature where ethene oligomerization is inhibited, only a negligible amount ($< 1\%$) of by-products (mainly C_3 – C_5 hydrocarbons) other than DEE are observed for all catalysts. H-EU-12 was found to give a lower initial products yield ($\approx 20\%$) than any of the other catalysts, probably owing to its highly elliptical 8-ring (2.7×5.0 and $2.8 \times 4.6 \text{ \AA}$) channel system (Table 1) that can limit, or temporarily restrict, the free diffusion of reactant molecules to the intrazeolitic acid sites. Among the eight cage-based small-pore catalysts compared, in addition, the initial ethene yield is larger in the order H-SAPO-34 \approx H-LTA $<$ H-SSZ-13(II) $<$ H-levyene $<$ H-SSZ-13(I) $<$ H-SSZ-39 \approx H-RTH(I) \approx H-RTH(II). Recall that the first four catalysts have no strong acid sites (Figure 3), suggesting that ethene formation requires strong acidity. This can be further supported by comparing the ethene yields of H-SSZ-13(I) and H-SAPO-34 with the same framework CHA topology, and also quite similar crystal sizes (Table 2), but different acidic properties (Figure 3).

An unexpected result from Figure 4 is that unlike the case of the other catalysts, the ethene yield over H-levyene gradually decreases over 10 h on stream. As described above, the acidity and crystal size of this LEV-type zeolite are quite similar to those of H-SAPO-34. Nevertheless, the amount (12.2 vs. 4.8 wt%) of organics deposited on the former catalyst during

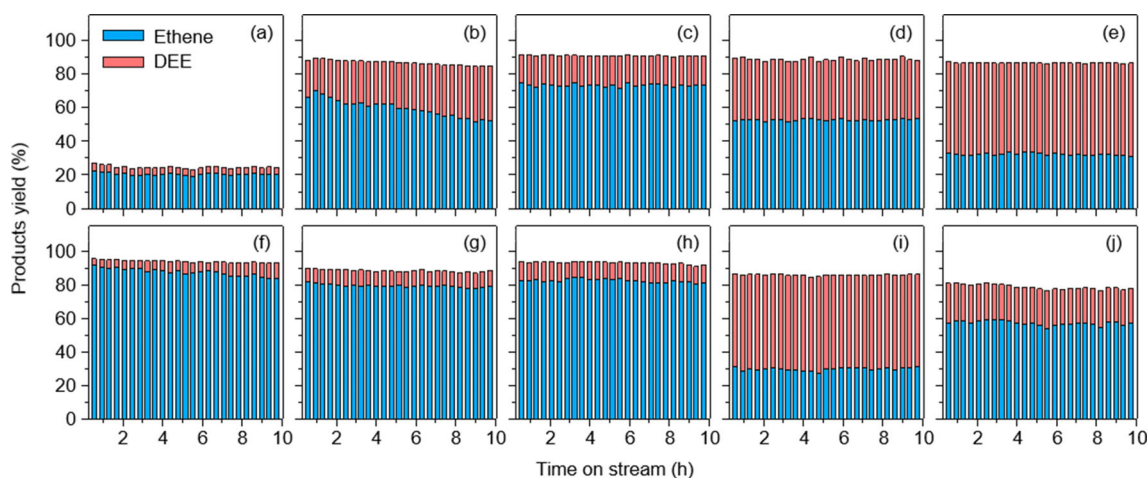


Figure 4. Yields of ethene and DEE as a function of TOS in ethanol dehydration over (a) H-EU-12, (b) H-levyene, (c) H-SSZ-13(I), (d) H-SSZ-13(II), (e) H-SAPO-34, (f) H-SSZ-39, (g) H-RTH(I), (h) H-RTH(II), (i) H-LTA, and (j) H-mordenite at 200°C under wet conditions ($\text{H}_2\text{O}/\text{EtOH} = 0.2$). The feed contains 5.9 kPa ethanol and 1.2 kPa water vapor with N_2 at 0.64 h^{-1} WHSV (EtOH).

ethanol dehydration at 200 °C and 0.64 h⁻¹ WHSV for 10 h is about 2.5 times larger than that on the latter catalyst (Table 2). The flushing experiments on the used H-levyne catalyst at the same temperature show that ethene is the only major species detected (Figure S3). However, even after flushing with N₂ (30 mL min⁻¹) for 10 h, the amount of organics in the resulting catalyst [determined by thermogravimetric and differential thermal analyses (TG/DTA)] is still high (9.6 wt%). It thus appears that most, if not all, of residual organics in flushed H-levyne may be DEE molecules that may not be prone to decompose to ethene under flushing conditions. This suggests that DEE production over this zeolite (Figure 4) is mainly catalyzed by the acid sites located on its crystal surface.

Given that the size of 8-ring windows is larger in H-levyne than in the other cage-based small-pore materials, the observed decrease in ethene yield of the former catalyst can be attributed to its *lev* cages that are considerably small compared with the cages in the other zeolite structure types (Table 1). We speculate that this may lead to a faster pore blockage of acid sites responsible for ethene formation, most likely by DEE. If such is the case, the cage volume of cage-based small-pore materials would then be a critical factor affecting the selectivity of the low-temperature dehydration of ethanol.

We have also examined the initial activities in ethanol dehydration over H-SSZ-13(I), H-SSZ-13(II), H-SSZ-39, H-RTH(I), and H-RTH(II) under wet conditions at temperatures lower than 200 °C, whose ethene yields are, to a certain degree, lower or higher than the ethene yield over H-mordenite at 200 °C. There is a thermodynamic limitation not only in the intramolecular dehydration of ethanol to ethene. Because of its endothermic nature, in addition, the decomposition of DEE into ethanol and ethene may not be easier at a lower temperature, as shown in Figure S4. Thus, it is clear that the optimal temperature for the efficient ethene formation from ethanol cannot be lower than 200 °C.

Figure 5 shows the long-term performance of five cage-based small-pore zeolites studied, as well as H-mordenite, at 200 °C and H₂O/EtOH = 0.2, but at a higher WHSV (1.92 h⁻¹).

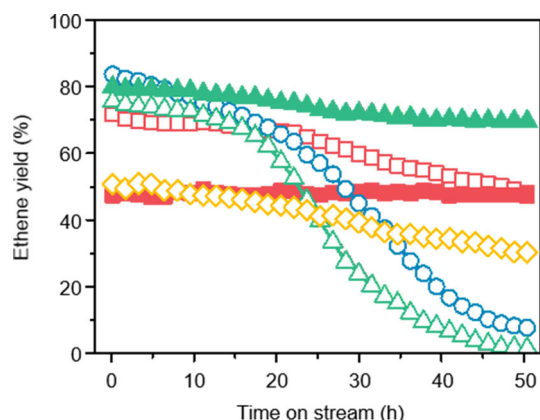


Figure 5. Long-term performance of H-SSZ-13(I) (□), H-SSZ-13(II) (■), H-SSZ-39 (○), H-RTH(I) (△), H-RTH(II) (▲), and H-mordenite (◇) for ethanol dehydration at 200 °C under wet conditions (H₂O/EtOH = 0.2). The feed contains 17.7 kPa ethanol and 3.6 kPa water vapor with N₂ at 1.92 h⁻¹ WHSV (EtOH).

Similar initial yields to those observed at a lower WHSV of 0.64 h⁻¹ (Figure 4) were obtained. However, unlike H-SSZ-13(I), H-SSZ-39, and H-RTH(I), which are all micro-sized, two nanocrystalline zeolites H-SSZ-13(II) and H-RTH(II) exhibit no significant decrease in ethene yield during 50 h on stream. This indicates that H-RTH(II) is the most active and stable among the catalysts studied here: its ethene yield (70%) becomes significantly higher than the yields of H-SSZ-13(I) and H-mordenite (48 and 31%, respectively) after 50 h on stream. As shown in Figure 5, in addition, both H-SSZ-39 and H-RTH(I) become almost completely deactivated. Therefore, it is clear that crystal size is the key to governing the durability of cage-based small-pore zeolites in ethanol dehydration. Most likely, nanocrystallinity shortens the diffusion length and thus slows the intrazeolitic accumulation of the bulky byproduct (i.e., DEE) that can block the acid sites. Despite the microcrystallinity, however, H-mordenite exhibits no significant decrease in ethene yield over the period of TOS. This can in our view be attributed to its 12-ring channels where the diffusion of reactant and (by)product molecules must be faster than that in cage-based small-pore materials, rendering H-mordenite more resistant to the accumulation of organics, probably of DEE (Figure S3). It is worth noting that when the used H-RTH(I) zeolite, which were completely deactivated during the long-term durability test (Figure 5), was regenerated by calcination in air at 550 °C for 8 h and then reacted with ethanol under the same conditions as those described above, it regained the initial activity (Figure S5). This suggests that the organics deposited are far from hard coke, revealing the high regenerability of our zeolite catalysts.

On the other hand, it is not difficult to infer that both 8-ring windows in the RTH framework (Table 1) are too narrow to allow the diffusion of DEE with a kinetic diameter of 5.4 Å,^[7b] without causing serious steric hindrance, like the case of H-levyne. Therefore, the selective ethene formation over an RTH-type zeolite cannot be rationalized in a way similar to that in H-mordenite. Transition-state shape selectivity is the only credible hypothesis to explain the suppression of the formation of ethanol dimers within the 8-ring side pockets in this large-pore zeolite.^[5b,11] Apparently, the cages in H-RTH would be considerably larger than even the 12-ring channels in H-mordenite (Table 1), easily allowing the formation of ethanol dimers and thus DEE molecules in this small-pore zeolite. This led us to conclude that its selective behavior for ethene formation can be rationalized by product shape selectivity. However, from a structural point of view, there is no reason only the RTH-type zeolite should be active and selective for low-temperature ethanol dehydration, explaining the high ethene yields observed for H-SSZ-13(I) and H-SSZ-39 (Figure 4).

In summary, we have demonstrated that nanocrystalline H-RTH is considerably more active and selective than any of the already known zeolitic catalysts for the low-temperature (200 °C) dehydration of ethanol to ethene in the presence of water vapor (H₂O/EtOH = 0.2). The overall results of our work suggest that its superior performance originates from a combination of the following factors: 1) cage volume and acid strength, which should be large and strong, respectively, enough to effectively catalyze the formation of DEE that subse-

quently decomposes to ethene; 2) cage window size, allowing the selective release of ethene produced; and 3) nanocrystallinity, reducing the diffusion path and thus slowing the blockage of intrazeolitic acid sites by DEE accumulation.

Acknowledgements

This work was supported by the National Creative Research Initiative Program (2012R1A3A2048833) through the National Research Foundation of Korea.

Conflict of interest

The authors declare no conflict of interest.

Keywords: biomass conversion · ethanol dehydration · nanocrystallinity · product shape selectivity · zeolites

- [1] a) J. Skupińska, *Chem. Rev.* **1991**, *91*, 613–648; b) D. Vogt in *Applied Homogeneous Catalysis with Organometallic Compounds, Vol. 8* (Eds.: B. Cornils, W. A. Herrmann), Wiley-VCH, Weinheim, **1996**, pp. 240–252; c) A. Forestière, H. Olivier-Bourbigou, L. Saussine, *Oil Gas Sci. Technol.* **2009**, *64*, 649–667.
- [2] a) S. K. Hoekman, A. Broch, C. Robbins, E. Ceniceros, M. Natarajan, *Renewable Sustainable Energy Rev.* **2012**, *16*, 143–169; b) R. A. Sheldon, *Green Chem.* **2014**, *16*, 950–963; c) A. Chierigato, J. V. Ochoa, F. Cavani in *Chemical and Fuels from Bio-Based Building Blocks, Vol. 1* (Eds.: ed. F. Cavani, S. Albonetti, F. Basile, A. Gandini), Wiley-VCH, Weinheim, **2016**, pp. 3–32.
- [3] a) M. R. Ladisch, K. Dyck, *Science* **1979**, *205*, 898–900; b) A. A. Kiss, D. J.-P. C. Suszwalak, *Sep. Purif. Technol.* **2012**, *86*, 70–78.
- [4] a) M. Zhang, Y. Yu, *Ind. Eng. Chem. Res.* **2013**, *52*, 9505–9514; b) D. E. Pearson, R. D. Tanner, D. Picclotto, J. S. Sawyer, J. H. Cleveland, Jr., *Ind. Eng. Chem. Prod. Res. Dev.* **1981**, *20*, 734–740; c) H. Adkins, P. P. Perkins, *J. Am. Chem. Soc.* **1925**, *47*, 1163–1167; d) E. G. Derouane, J. B. Nagy, P. Dejafive, J. H. C. van Hooff, B. P. Spekman, J. C. Védrine, C. Naccache, *J. Catal.* **1978**, *53*, 40–55; e) P. Vázquez, L. Pizzio, C. Cáceres, M. Blanco, H. Thomas, E. Alesso, L. Finkielstein, B. Lantaño, G. Moltrasio, J. Aguirre, *J. Mol. Catal. A* **2000**, *161*, 223–232.
- [5] a) I. Takahara, M. Saito, M. Inaba, K. Murata, *Catal. Lett.* **2005**, *105*, 249–252; b) H. Chiang, A. Bhan, *J. Catal.* **2010**, *271*, 251–261.
- [6] J. Bae, J. Cho, J. H. Lee, S. M. Seo, S. B. Hong, *Angew. Chem. Int. Ed.* **2016**, *55*, 7369–7373; *Angew. Chem.* **2016**, *128*, 7495–7499.
- [7] a) S. Aguado, G. Bergeret, C. Daniel, D. Farrusseng, *J. Am. Chem. Soc.* **2012**, *134*, 14635–14637; b) D. Ben-Amotz, K. G. Willis, *J. Phys. Chem.* **1993**, *97*, 7736–7742.
- [8] K. Alexopoulos, M. John, K. Van der Borght, V. Galvita, M.-F. Reyniers, G. B. Marin, *J. Catal.* **2016**, *339*, 173–185.
- [9] a) B. Han, S.-H. Lee, C.-H. Shin, P. A. Cox, S. B. Hong, *Chem. Mater.* **2005**, *17*, 477–486; b) S. I. Zones, US 4544538, **1985**; c) Z. Li, M. T. Navarro, J. Martínez-Triguero, J. Yu, A. Corma, *Catal. Sci. Technol.* **2016**, *6*, 5856–5863; d) H. Van Heyden, S. Mintova, T. Bein, *Chem. Mater.* **2008**, *20*, 2956–2963; e) M. Dusselier, J. E. Schmidt, R. Moulton, B. Haymore, M. Hellums, M. E. Davis, *Chem. Mater.* **2015**, *27*, 2695–2702; f) D. Jo, G. T. Park, J. Shin, S. B. Hong, *Angew. Chem. Int. Ed.* **2018**, *57*, 2199–2203; *Angew. Chem.* **2018**, *130*, 2221–2225; g) D. Jo, J. B. Lim, T. Ryu, I.-S. Nam, M. A. Cambor, S. B. Hong, *J. Mater. Chem. A* **2015**, *3*, 19322–19329; h) D. Jo, T. Ryu, G. T. Park, P. S. Kim, C. H. Kim, I.-S. Nam, S. B. Hong, *ACS Catal.* **2016**, *6*, 2443–2447.
- [10] Ch. Baerlocher, L. B. McCusker, Database of Zeolite Structures: <http://www.iza-structure.org/databases/> (accessed Apr 20th, 2018).
- [11] T. K. Phung, L. P. Hernández, A. Lagazzo, G. Busca, *Appl. Catal. A* **2015**, *493*, 77–89.

Manuscript received: April 20, 2018

Revised manuscript received: May 14, 2018

Version of record online: ■ ■ ■ 0000

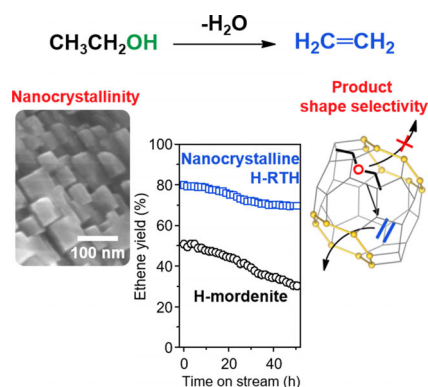
COMMUNICATIONS

J. H. Lee, S. Lee, S. B. Hong*

■ ■ - ■ ■



VIP Nanocrystalline H-RTH Zeolite: An Efficient Catalyst for the Low-Temperature Dehydration of Ethanol to Ethene



Selective and robust! Efficient dehydration of bioethanol to ethene is catalyzed by nanocrystalline H-RTH zeolite. Whereas the zeolite cage volume and window size, as well as acid strength, play a key role in the selective formation of ethene, its nanocrystalline nature is responsible for its superior durability.